

# Engine-out emissions from a modern high speed diesel engine – the importance of Nozzle Tip Protrusion

Felix Leach<sup>1†</sup>, Riyaz Ismail<sup>1</sup>, Martin Davy<sup>1</sup>

1. Department of Engineering Science, University of Oxford, Oxford, UK

† Corresponding author: felix.leach@eng.ox.ac.uk

## Abstract

Engine out emissions from a diesel engine are highly dependent on the nature of the fuel/air interactions in cylinder, which in turn depend on the detail of the fuel injection process. High temperatures, which promote soot oxidation, also promote NO<sub>x</sub> formation. Carefully controlling these interactions can lead to cleaner combustion resulting in lower engine-out emissions, thus reducing the burden on the aftertreatment system. In this work a minor (0.5 mm) variation in injector Nozzle Tip Protrusion (NTP) is tested, both experimentally and numerically, at two part-load and four full-load test points. The results indicate that a 0.5 mm variation in NTP can have a significant benefit in reducing soot emissions, across the engine operating map, whilst not having an impact on other emissions or fuel consumption. This paper demonstrates the practical importance of NTP, and demonstrates the sensitivity of engine-out emissions to relatively minor variations of this key element of the combustion system geometry which might occur naturally either in production or in service.

Keywords: Spray targeting, Diesel Combustion, NO<sub>x</sub>, Soot, NTP

## Introduction

Diesel engines are seen as a key pathway towards reducing CO<sub>2</sub> emissions from hydrocarbon fuelled powertrains – diesel powered light-duty vehicles emit up to 20 % less CO<sub>2</sub> than gasoline equivalents [1]. In 2017, 42 % of all light duty vehicles (including those with hybrid and electric powertrains) sold in the UK were powered by diesel powertrains [2] while light duty vehicles with diesel engines made up 49 % of all registrations in the EU [3]. The modern diesel engine, coupled with a

matched aftertreatment system, emits very low levels of pollutants at the tailpipe; however, the required aftertreatment devices add significant complexity and cost (around \$1500 [4]) to a vehicle. Additionally, there are costs, in terms of engine efficiency, fuel economy, and maintenance associated with the operation of the aftertreatment systems through the lifetime of the vehicle.

The aftertreatment system on a modern diesel vehicle typically includes a Diesel Particulate Filter (DPF) for soot and Particulate Matter (PM) control, a Diesel Oxidation Catalyst (DOC) for hydrocarbon removal and some form of NO<sub>x</sub> catalyst. Usually DPFs have a filtration efficiency of > 99 % after a few minutes of soot loading. However, soot loading increases the flow resistance in the DPF by a few kPa, which, in turn, increases the pumping work of the engine and reduces engine efficiency [5]. As a result, DPFs require periodic regeneration to clean (via oxidation) the trapped soot/PM from the substrate. Typically, DPF regeneration is achieved by operating the engine with increased exhaust temperature – thus incurring a fuel economy penalty of 1-3 % [6].

NO<sub>x</sub> emissions may be controlled using either a Lean NO<sub>x</sub> Trap (LNT) catalyst, Selective Catalytic Reduction (SCR), or a combination of the two [7]. LNTs are typically 70-90 % efficient, and work by trapping NO<sub>x</sub> on the catalyst which is then catalytically reduced by hydrocarbons during engine rich operation. This periodic rich operation to regenerate the LNT typically incurs a fuel consumption penalty of 5 % [8]. SCR reduces NO<sub>x</sub> to nitrogen and water in the presence of ammonia. SCRs require a supply of Diesel Exhaust Fluid (DEF) – an aqueous solution of urea – meaning an extra tank and injection equipment is required on vehicle as well as additional monitoring. Efforts to reduce the capital and operating cost of diesel aftertreatment systems, through reducing engine out emissions, are therefore of importance if diesel engines are to continue to contribute reducing CO<sub>2</sub> from the light-duty fleet.

It is well understood that engine-out emissions (i.e. before any aftertreatment) from diesel engines are highly dependent on the detail of the interaction between the fuel being injected and the air in-cylinder at injection. Combustion initiates in zones that are locally fuel rich (overall the mixture in-cylinder is typically lean) and at relatively low temperatures (as combustion is just beginning) causing large quantities of soot to be generated. Much of this soot is subsequently oxidized in the diffusion phase of combustion, which occurs at higher temperatures. These higher combustion temperatures lead to the formation of NO<sub>x</sub>.

It is also well established that greater air entrainment into the diesel spray at injection will lead to a reduction in soot emissions and an improvement in efficiency, as there will be more oxygen available to oxidise the fuel completely [9], but that this greater air entrainment typically leads to an increase in NO<sub>x</sub> as combustion temperatures are higher and there is more oxygen available to react with nitrogen [11]. Commonly, such air/fuel mixing is improved by using high fuel injection pressures (promoting spray atomization) and the use of multiple injections (entraining air into the fuel jet) . In addition, it has been shown that the interaction of the fuel spray with motion of the charge in-cylinder and combustion chamber

geometry will have a significant impact on the fuel/air mixing due to air entrainment [15, 17]. This occurs regardless of the method of changing the fuel/air mixing whether injector technology [16] or in conventional or low temperature combustion [18].

In any modern diesel engine the final design must ensure that the fuel/air interactions on injection lead to low emissions without compromising performance. In production, designers must also consider robustness against deviations from the ideal, for example due to manufacturing tolerances. Fuel spray targeting is often controlled by adjusting fuel injector nozzle tip protrusion (NTP) or spray angle. Miles and Andersson [19] state that NTP itself is not often studied directly, rather as a calibration parameter for differing spray angles, but note that deeper NTP is likely to increase injector tip temperature. NTP is often mentioned as a calibration parameter [20-22], for example Tonetti *et al.* discuss calibrating with NTP in their work [22], however comprehensive studies of the effect of NTP are rare. Given that this is a parameter which could be sensitive enough to be affected by manufacturing tolerances, or changed during a vehicles service life (for example during a fuel injector change) there is a need to explore in depth the impact of NTP in a modern diesel engine.

In this work we investigate the emissions and performance of a modern light-duty high-speed diesel engine when varying NTP. The NTP is changed by 0.5 mm (an extremely minor change) using a conventional re-entrant bowl shape. Results from physical experiments are supported by 3-dimensional numerical modeling studies performed in commercially available CFD package. The simulation results are used to understand what is causing the results seen in the physical experiments.

## Experimental Method

A comprehensive discussion of the experimental set-up both for the physical experiments and the CFD simulations is included in the authors' recent papers [20, 23]; a brief summary is included here for convenience.

## Engine

A single cylinder Ricardo Hydra diesel engine fitted with a modern high speed diesel engine cylinder head was used in this work. The test cell and engine have been fully described in previous publications [24]. Some important engine parameters are shown in Table 1. The engine was run on a standard BS EN 590 diesel fuel [25].

**Table 1: Specifications of the single-cylinder engine**

Bore $\times$ Stroke	83 $\times$ 92.4 mm
Displacement	500 cm <sup>3</sup>
Valves per Cylinder	2 intake, 2 exhaust
Compression Ratio	15.4 : 1
Fuel Pressure	400-1800 bar
Injector	DI common rail

## Instrumentation

The instrumentation used in this work has been previously described in [26]. Of note is that cooled high pressure EGR is used alongside an external boosting rig and exhaust back pressure control; all emissions are measured using standard instrumentation on an engine-out basis – the engine is not fitted with a turbocharger or catalyst. A standard (EN590) B0 test diesel was used [25]. A schematic of the test facility is shown in Figure 1.

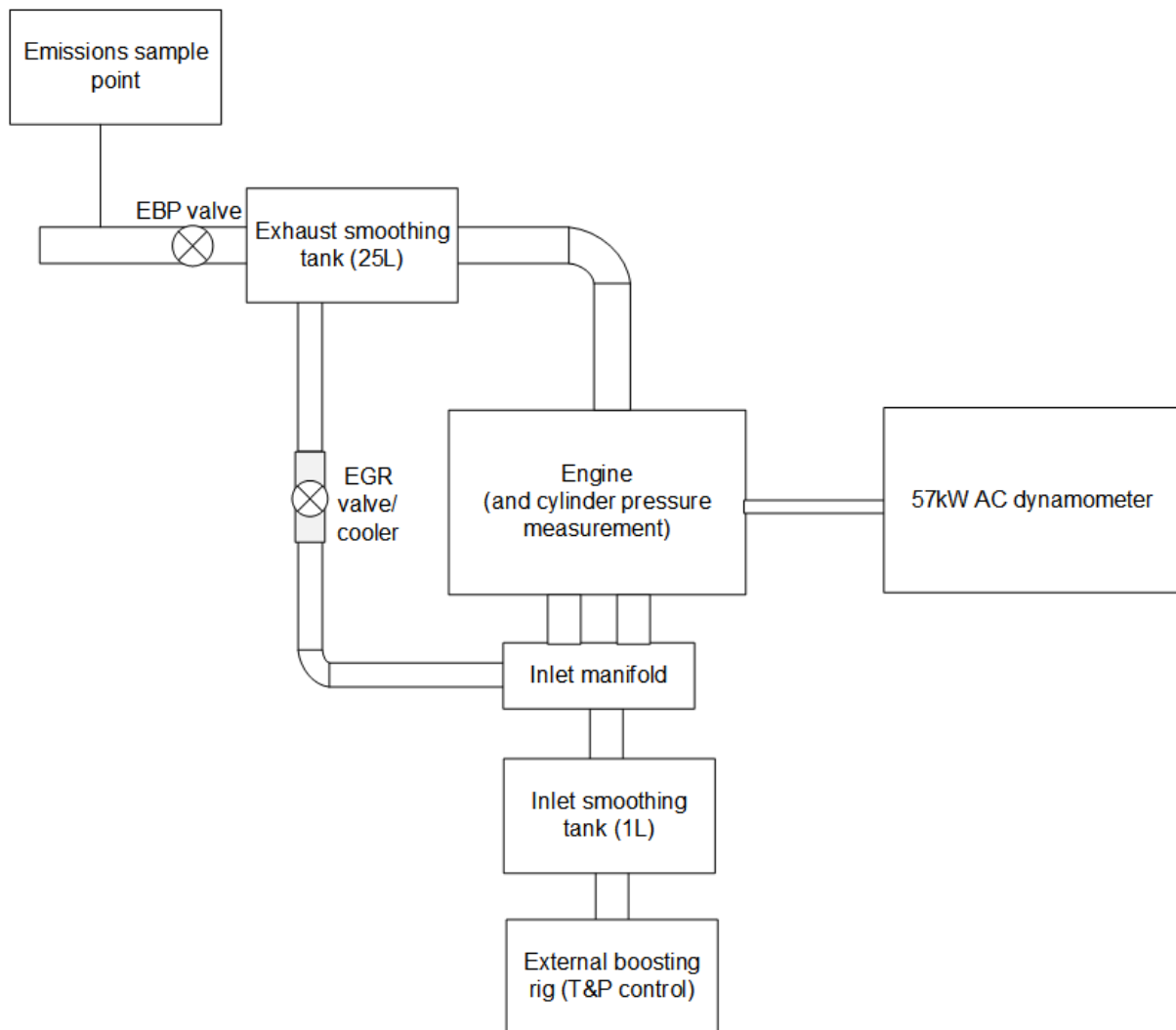


**Figure 1: Test cell schematic. Adapted from [26].**

Indicated specific fuel consumption (ISFC) measurements are calculated using fuel flow from a gravimetric system and IMEP as derived from a Kistler high speed in-cylinder pressure sensor. ISFC was calculated based on a mean of 10 s samples of fuel flow over three minutes, using a periodically updating IMEP from the AVL indiset combustion analyser. This gives an accuracy in ISFC at the most demanding condition (1500 rpm/6.8 net IMEP) of  $\pm 1.5\%$  and at the least demanding conditions (highest fuel flow rates and IMEPs) of  $\pm 0.35\%$ .

## CFD – model & validation

A commercial CFD code was used for all simulations [27], and detail of the computational setup used in this investigation has been reported in [20]; so only a brief overview will be given. The CFD code and models used have been validated extensively through the Engine Combustion Network (ECN) spray experiments for both non-reacting [28] and reacting [29] conditions.

The ECFM-3Z model coupled with tabulated kinetic ignition (TKI) was used for combustion modelling [30], which has been validated for high speed direct injection (HSDI) diesel engines of this type in [31]. N-heptane was used as a surrogate fuel with the Chalmers mechanism (42 species, 168 reactions) used for computation of the TKI tables. Further information about the TKI model and its applicability to HSDI engines can be found in [31]. Turbulence closure was accounted for through the well-known RNG-k-epsilon model [32] with heat transfer to the walls being modelled with the Han & Reitz model [33]. The discrete droplet methodology was used to simulate the liquid phase with spray injection and breakup modelled by the Reitz-Diwakar [34] and KH-RT [35] models. Additionally, dynamic droplet drag [36], NTC collisions [37] and the Frossling correlation [38] were used to model droplet drag, collisions and vaporisation.

The computational domain was limited to a 45 degree sector of the engine cylinder only simulating a single nozzle of the equispaced injector. The computational mesh had a nominal base cell size of 1.4 mm with cell refinement (0.175 mm cell size) in the near nozzle region and adaptive mesh refinement (0.175 mm cell size) applied to regions of high velocity and temperature gradients. The simulations were run from just after IVC to before EVO. In-cylinder conditions were initialised with experimental pressure measurements. Wall temperatures were fixed for each simulation and fuel injection rates for each test point were generated from a 1D dynamic model of the injector. NO formation was modelled with the Extended Zeldovich Mechanism [39] and the Hiroyasu empirical model was used to model soot formation, with Nagle and Strickland-Constable model for soot oxidation [40, 41]. A comprehensive description of the model and recommended model constants can be found in [27].

The CFD model was validated at 0 % EGR with NTP 1; again a comprehensive overview of the validation is described in [23]. Figure 2 shows the comparison between the cylinder pressure and heat release traces from the experimental data and the CFD predictions at full load / 2000 rpm; an excellent match is observed albeit with a minor differences. The difference in pilot burn at around -20 CAD is attributed to the uncertainty in the injection rate from the 1D model (the pilot makes up 1.7 % of the total mass of fuel injected at this test point) as well as uncertainties in the combustion model, which uses simplified chemistry which may mean the low temperature heat release associated with the pilot is incorrectly captured. There is a notable difference in instantaneous heat release at around 20 CAD. This is attributed to the fact that at around 14 CAD corresponds to the time of maximum mass flow rate through the injector; consequently, fuel impingement at this point is considerable. The spike seen in instantaneous heat release thereafter is attributed to this impinged fuel now burning.

There is also a slight under-prediction in the final value of the cumulative heat release and in the instantaneous heat release after 45 CAD. This is attributed to uncertainty in wall temperatures, and the choice of heat transfer model.

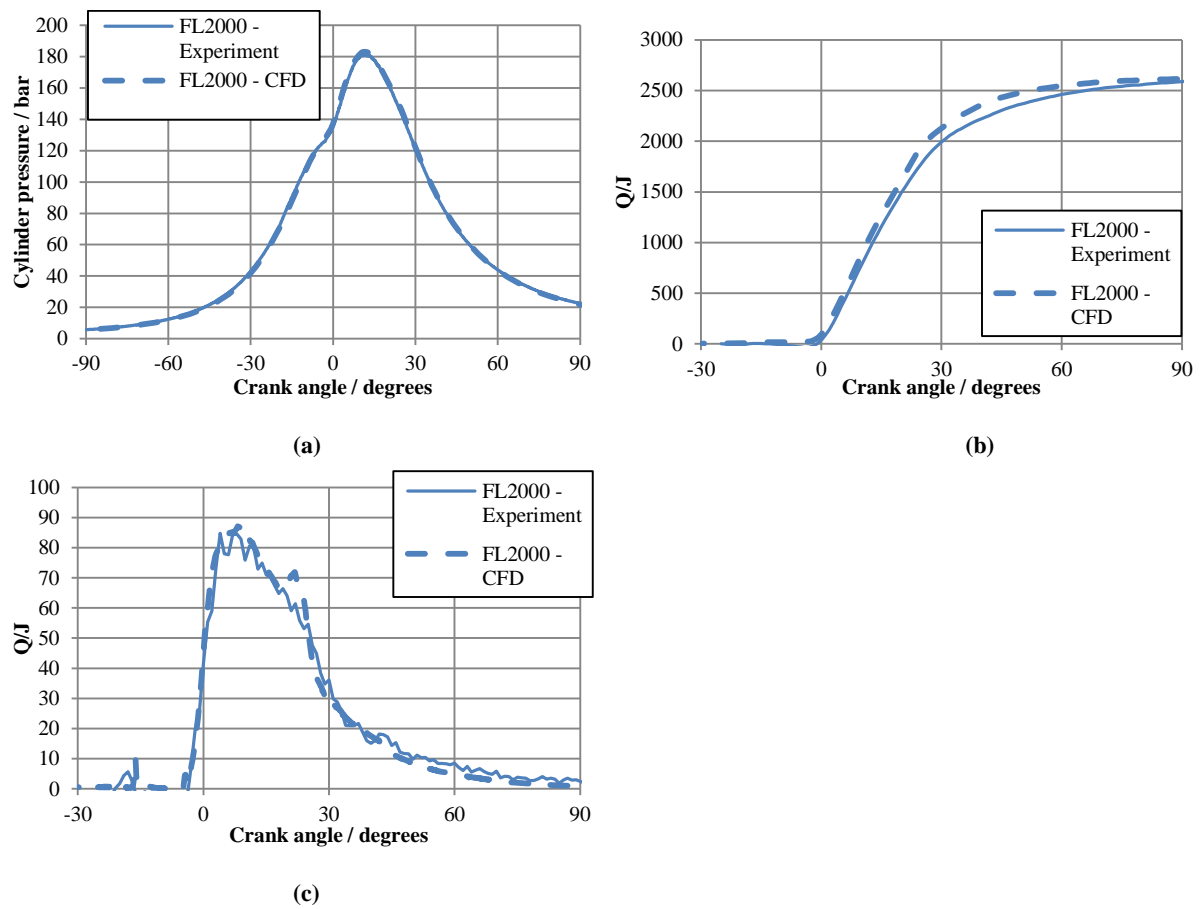


Figure 2: Comparison between experimental and CFD cylinder pressure traces (a), cumulative heat releases (b), and instantaneous heat release (c).

## Results and discussion

The engine was run and simulated in CFD at two part load steady state speed/load operating points, 6.8 bar net IMEP and 13.5 bar net IMEP at several EGR levels as details in Table 2. The engine was also run at full load at four engine speeds without EGR. The injection timing (consisting of a small, fixed pilot, and a single main injection) remained fixed for each test point. The IMEP was set by varying the main injection quantity only; IMEP was held constant at each test point. At full load the injected fuel quantity was limited by exhaust temperature (810 °C) and the injection advance was limited by peak cylinder pressure (180 bar). NTP was varied by changing the position of the injector tip 0.5 mm in the combustion chamber using sealing washers of different thickness on the base of the injector.

Table 2: Engine test conditions

Test point ID	1500/6.8	1750/13.5	FL1500	FL2000	FL3000	FL4000
---------------	----------	-----------	--------	--------	--------	--------

Engine speed (rpm)	1500	1750	1500	2000	3000	4000
Net IMEP (bar)	6.8	13.5	Max <sup>†</sup>			
Inlet manifold pressure (barG)	0.25	1.0	1.55	1.85	1.95	1.65
Exhaust back-pressure (barG)	0.45	1.4	1.9	1.75	2.4	2.5
Inlet air temperature (°C)	Dependant on EGR		40	45	50	50
Coolant and oil temperature (°C)	90					
EGR level(Approx.)	0-40%	0-27%	0			
Fuel rail pressure (MPa)	55	90	110	145	180	180

<sup>†</sup>Maximum IMEP limited by peak cylinder pressure and maximum exhaust temperature

For reasons of commercial confidentiality, all emissions and fuel consumption readings have been rescaled by dividing by a nominal value – the same nominal value for all load points. All of the data is presented against ISNO<sub>x</sub>, acting as an indicator of the external EGR levels with values closest to 1 indicating no EGR, and values closest to 0 indicating the maximum level of EGR tested.

## Part load results

The part load results from this work have been reported in a previous publication by the authors [24]. Here we will use the CFD analysis to understand and explain the trends observed in that work. The validated CFD model was used to run simulations at all experimental test points with variations in NTP and EGR rate. Additionally, the fuel rate was adjusted for each simulation in order to best match the target IMEP at that test point.

Figure 3 and Figure 4 show the NO<sub>x</sub>-Soot emissions across the EGR range for both NTPs at the two part load test points. A good agreement between experiment and simulation can be seen with the emissions trends being captured correctly for both test points. It should be noted that part of the deviations in results between experiment and simulation can be attributed to the variations in experimental EGR rate away from the nominal target EGR. From Figure 3 and Figure 4, it can be seen that NTP 2 has a beneficial NO<sub>x</sub>-soot trade-off compared to NTP 1 across the EGR range at both test points with a significant overall reduction in soot and a marginal increase in NO<sub>x</sub> at high levels of EGR.

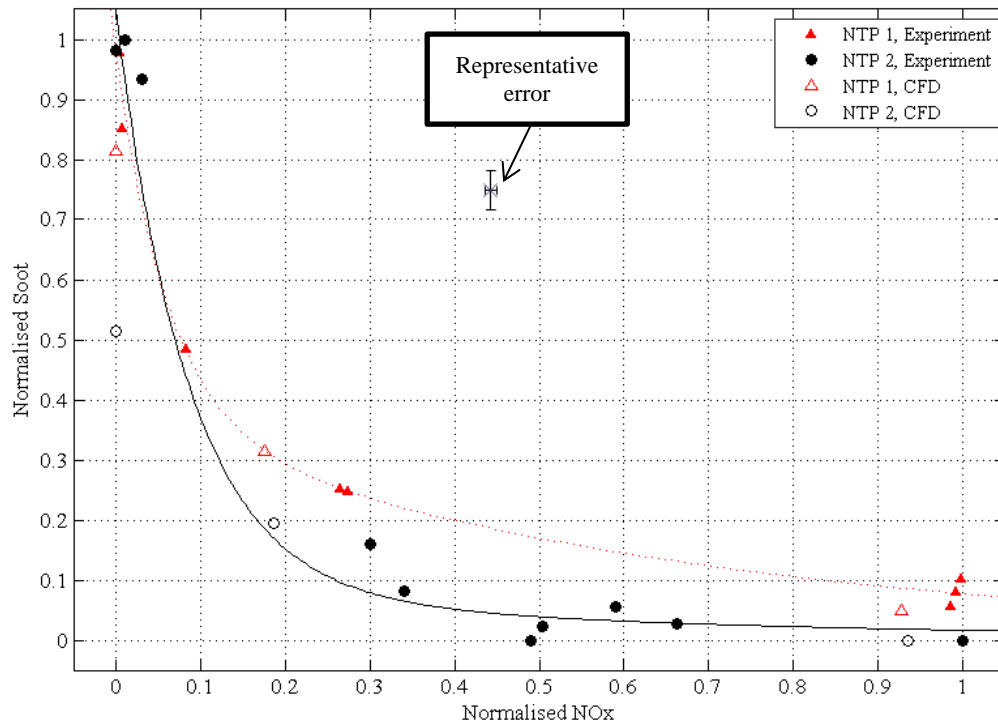


Figure 3: Normalised NO<sub>x</sub>-soot tradeoff at 1500/6.8 showing both experimental results and the prediction from CFD. NB experimental NO<sub>x</sub> in ppm, CFD NO<sub>x</sub> in kg, experimental soot in FSN, CFD in kg. The solid line (NTP 1) and dotted line (NTP 2) are lines of best fit. For clarity, a representative error of  $\pm\sigma$  for the experimental data is shown

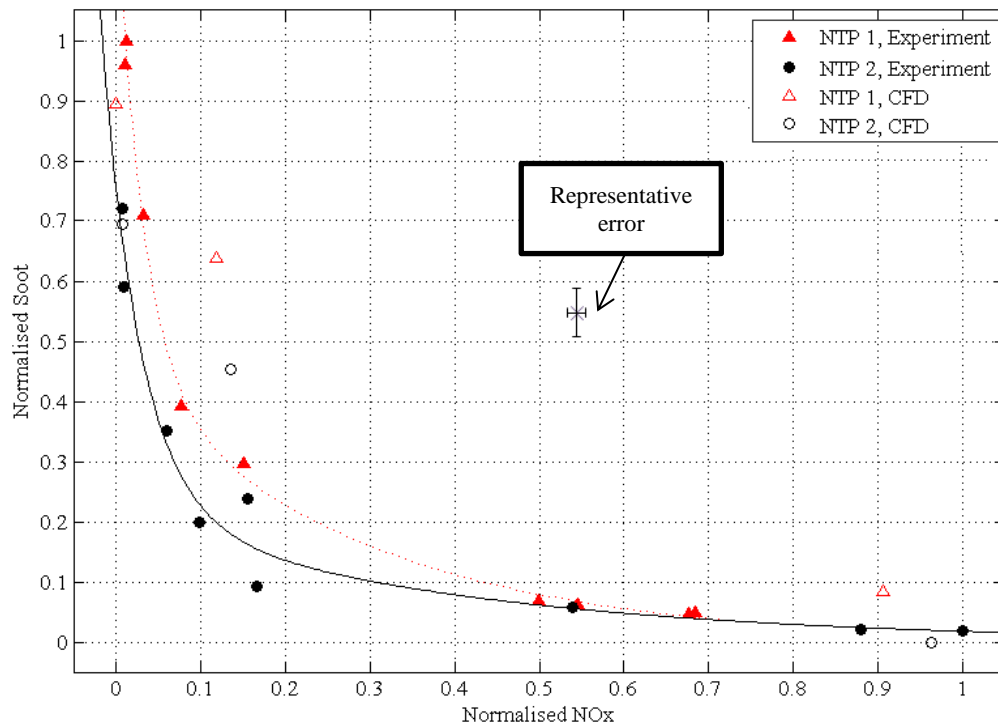
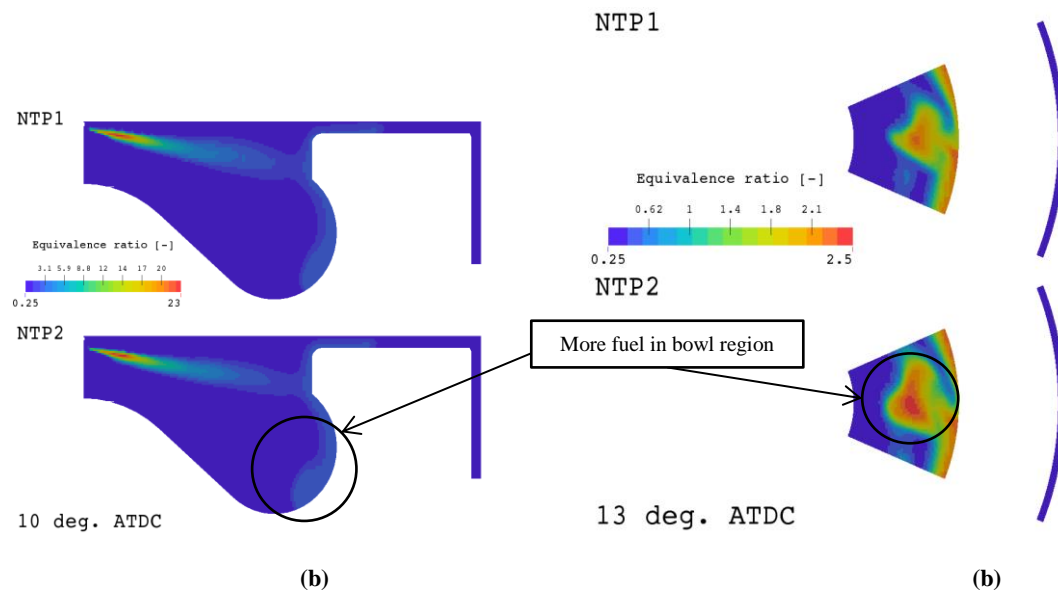


Figure 4: Normalised NO<sub>x</sub>-soot tradeoff at 1750/13.5 showing both experimental results and the prediction from CFD. NB experimental NO<sub>x</sub> in ppm, CFD NO<sub>x</sub> in kg, experimental soot in FSN, CFD in kg. The solid line (NTP 1) and dotted line (NTP 2) are lines of best fit. For clarity, a representative error of  $\pm\sigma$  is shown



The reason for this improved NO<sub>x</sub>-Soot trade-off achieved with NTP 2 can be seen in Figure 5a; the effect of NTP 2 is to split the spray jet more towards the bowl than the fire-land. The spray momentum is then able to force more fuel into the bowl region and away from the piston walls which in turn improves air entrainment and mixing. This can be seen in Figure 5b and Figure 6 where there is a greater area of high velocity air in the bowl for NTP 2 as well as the equivalence ratio distribution being toward the piston crown. Consequently, there are less fuel rich regions especially along the piston wall resulting in lower soot formation as shown in Figure 7a. Additionally, as less fuel penetrates into the fire-land region at NTP 2, spray impingement on the piston walls is reduced leading to fewer locally rich regions on the surface of the piston thereby discouraging soot formation. This is clearly seen in Figure 7b where soot concentration on the piston wall is much higher at NTP 1.



**Figure 5: Predicted equivalence ratio distribution X-Z (a) and X-Y (b) plane comparing NTP 1 (upper) and 2 (lower), 40% EGR at 1500/6.8.**

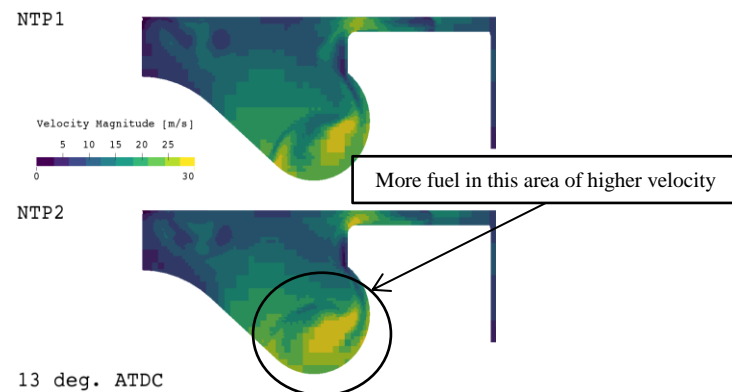


**Figure 6: Predicted velocity field X-Z plane for NTP 1 (upper) and 2 (lower), 40% EGR at 1500/6.8.**

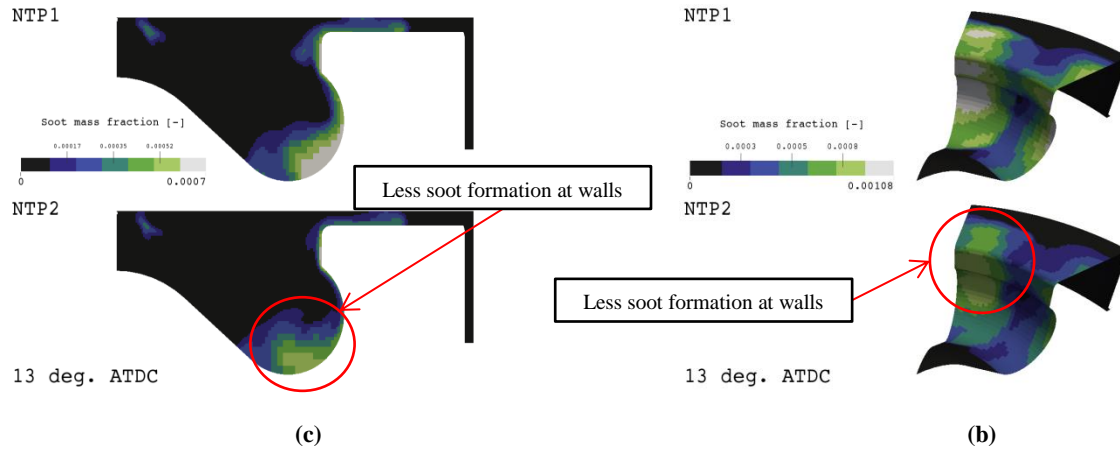


**Figure 7: Predicted soot mass fraction distribution for NTP 1 (upper) and 2 (lower), X-Z plane (a) and 3D visualization (c), 40% EGR, at 1500/6.8.**

The formation and oxidation rates of soot can be studied to give a better understanding of the reduction in soot across both part load test points from NTP 2. Plotted in Figure 8 and Figure 9 is the soot formation, oxidation and cumulative soot mass at the highest EGR rate at both part load test points. It can be seen that at the lower load test point (Figure 8), moving from NTP 1 to NTP 2 leads to a significant reduction in soot formation as well as a less significant decrease in soot oxidation. At this lower load test point the rate of soot oxidation is proportional to the soot concentration so the reduction in overall soot leads to a commensurate reduction in soot oxidation. This results in a significant net decrease in soot mass. On the other hand, at higher load (Figure 9), moving from NTP 1 to NTP 2 decreases soot formation very slightly however the relatively more significant increase in soot oxidation is the principle mechanism of overall soot reduction at this higher load test condition – a completely different mechanism of soot reduction to at the light load test point.

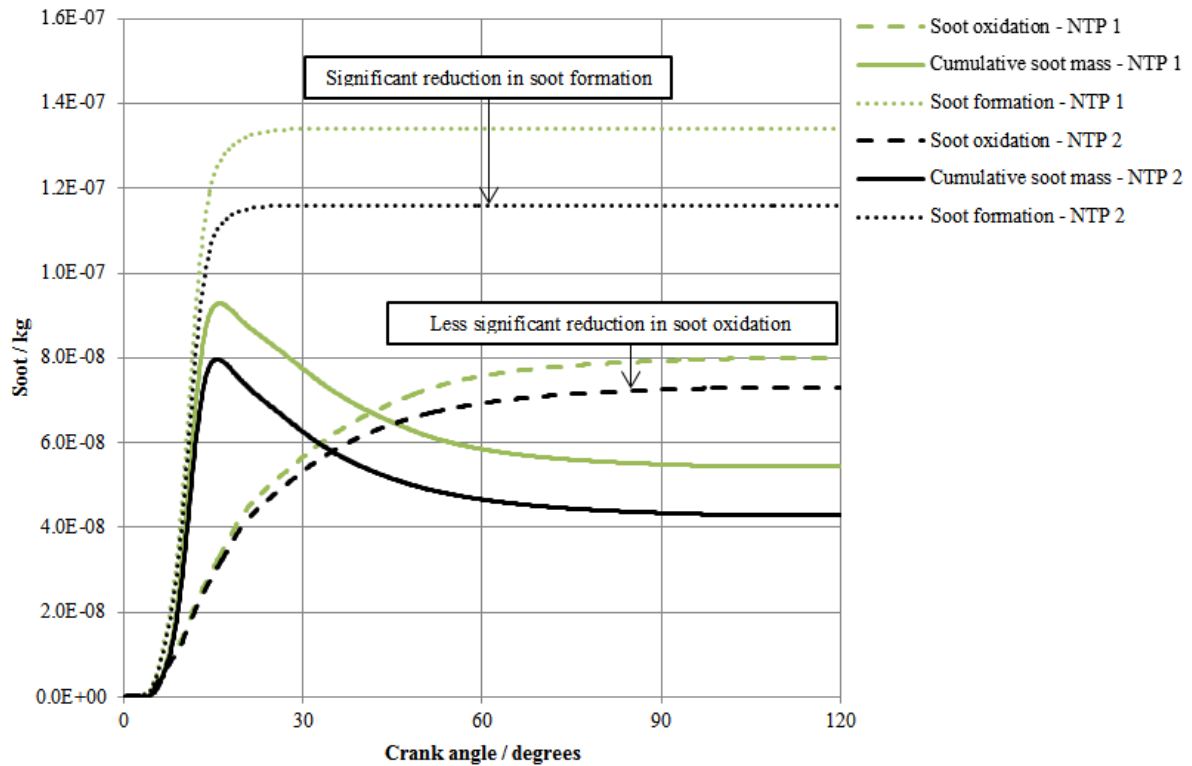


Figure 8: Predicted soot formation, oxidation and cumulative mass through the combustion phase for both NTPs at 1500/6.8.

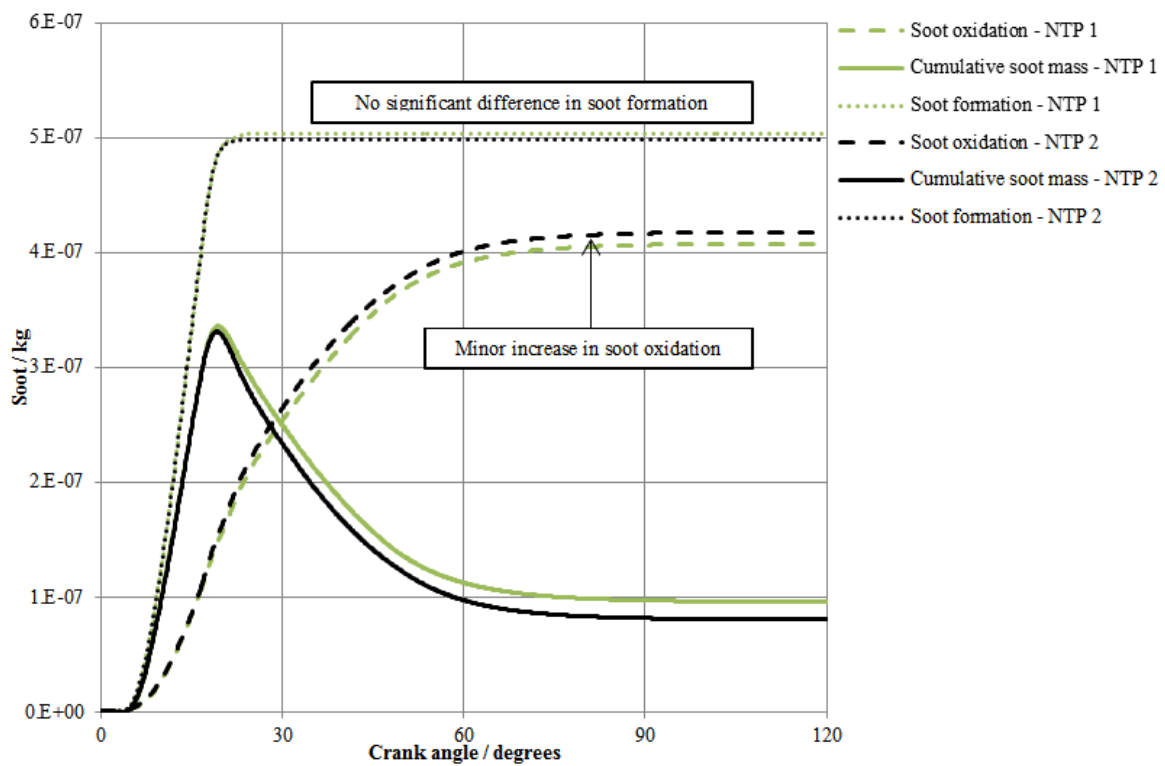


Figure 9: Predicted soot formation, oxidation and cumulative mass through the combustion phase for both NTPs at 1750/13.5.

## Full load results

The full load operating points were run at four engine speeds (1500, 2000, 3000, and 4000 rpm) – with full load defined as the maximum fuel injection advance possible while remaining below the maximum cylinder pressure sustainable and with the maximum fuel quantity injected while remaining below the maximum exhaust temperature permitted (810 °C). Main injection angle varied between NTPs by less than 0.5 CAD for all full load operating points. The engine operating parameters were shown in Table 2. Figure 10a shows the smoke emissions (FSN) from the engine at full load. In general the trends seen at part load hold here at full load, with NTP 2 giving a decrease in soot emissions. The CFD predictions of soot mass are shown in Figure 10b. There is general agreement between these results and those from the physical experiments. However, it is not possible to make absolute comparisons between the two sets of results as the CFD model predicts the soot mass in cylinder as the exhaust valve opens, whereas the experimental results are measured some way downstream of the exhaust valve, using a smoke meter, which measures the soot collected on a filter paper using the FSN method. In particular, this accounts for the higher soot mass predicted at 4000 rpm which is not observed in the experimental results, as there will be significant post flame oxidation (with exhaust temperatures over 810 °C as shown in Figure 11) which is not accounted for in the CFD model at all. Both the soot predictions and measured FSN results show a reduction in soot mass and FSN with NTP 2.

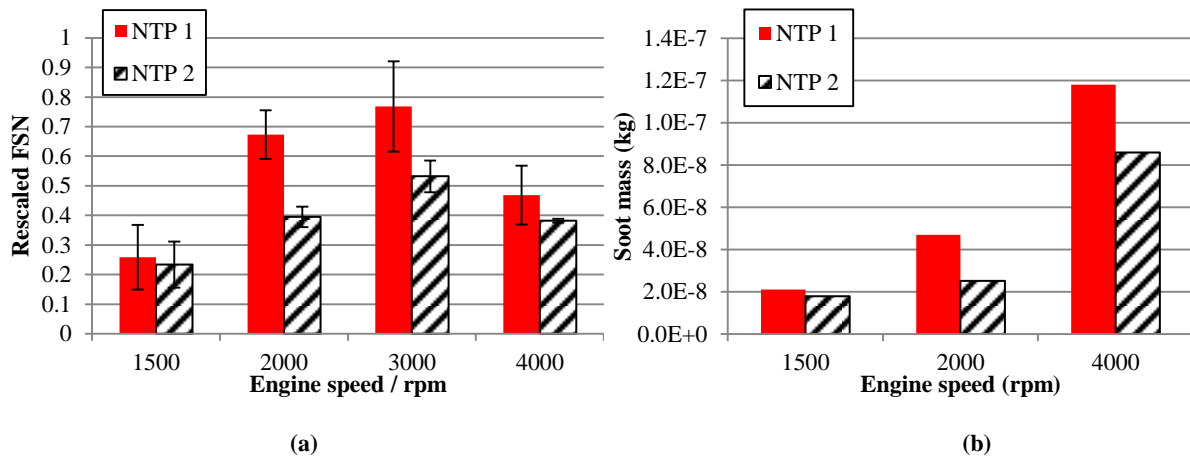


Figure 10: Measured FSN emissions (a) and CFD predicted soot mass (b) at full load. The error bars correspond to  $\pm\sigma$ .

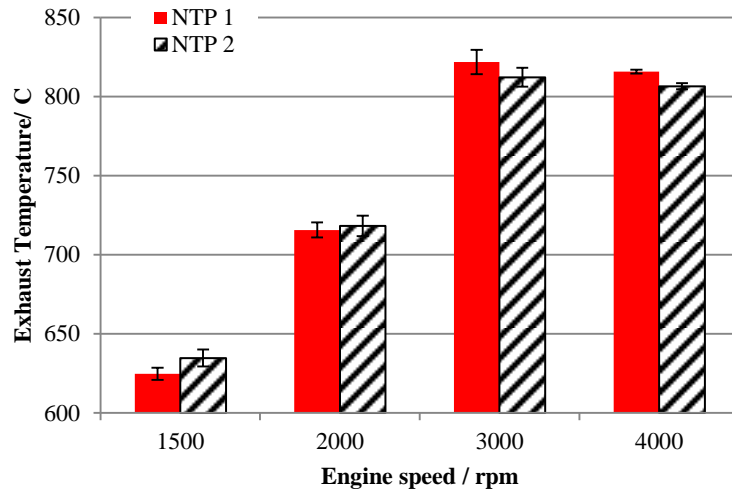
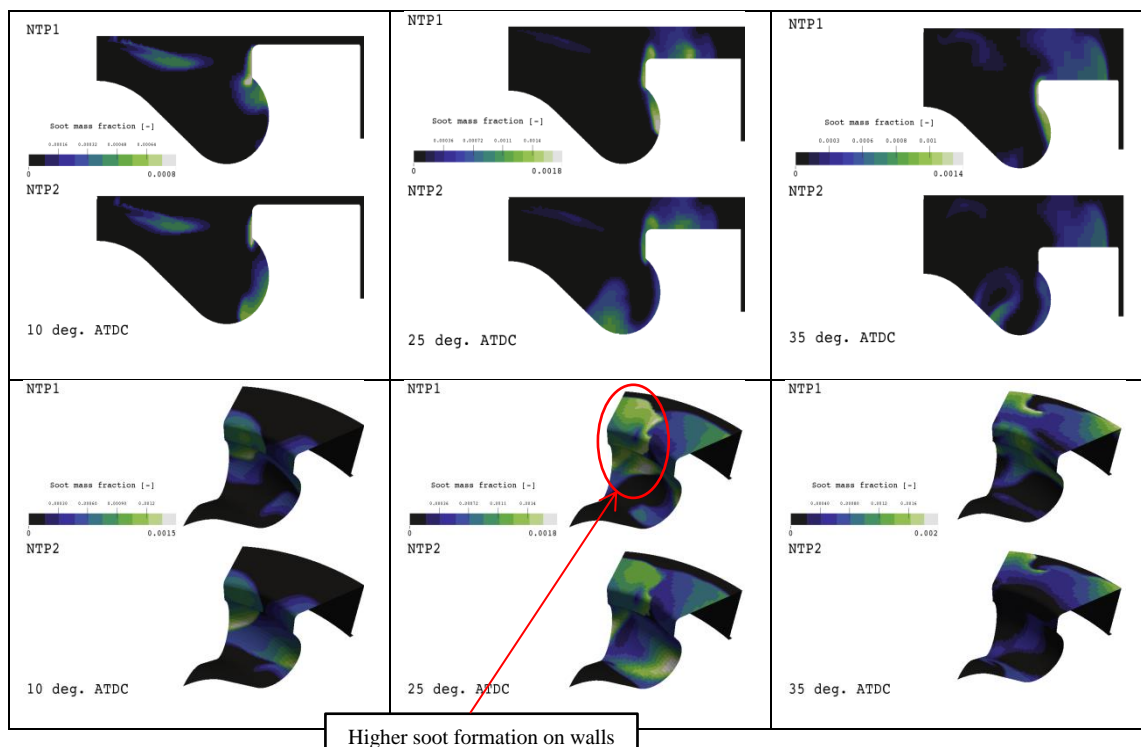
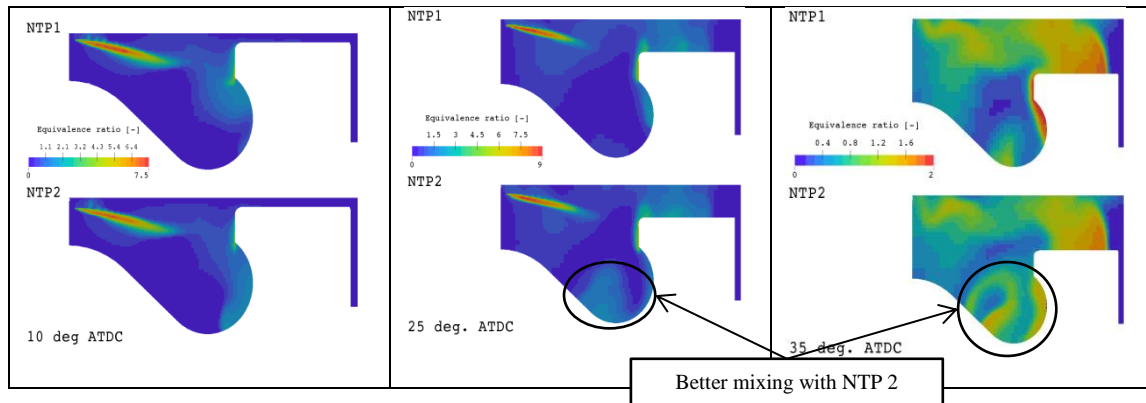


Figure 11: Exhaust temperatures at full load. The error bars correspond to  $\pm\sigma$ .

Examining the CFD and soot evolution through the cycle it is possible to understand why these results are occurring. As an example, at 4000 rpm there is a clear reduction in soot when moving from NTP 1 to NTP 2. Figure 12 shows the in-cylinder soot mass fraction at three crank angles, it can be seen that 25 CAD, NTP 1, there is significant soot formation in the fire land, which is reduced with NTP 2, as might be expected – the fuel and air is mixing more in the bowl with the deeper NTP, this can be seen in Figure 13, where, due to the air motion and bowl vortex, the equivalence ratio in the bowl can be seen to be significantly lower in the bowl, showing more oxygen availability for complete combustion. In addition there are higher temperatures seen within the bowl (Figure 14) which will be promoting soot oxidation.



**Figure 12: Predicted in-cylinder soot mass fraction at three crank angles for NTP 1 (upper) and NTP 2 (lower) at 4000 rpm.**



**Figure 13: Predicted equivalence ratios in cylinder at three crank angles for NTP 1 (upper) and NTP 2 (lower) at 4000 rpm.**

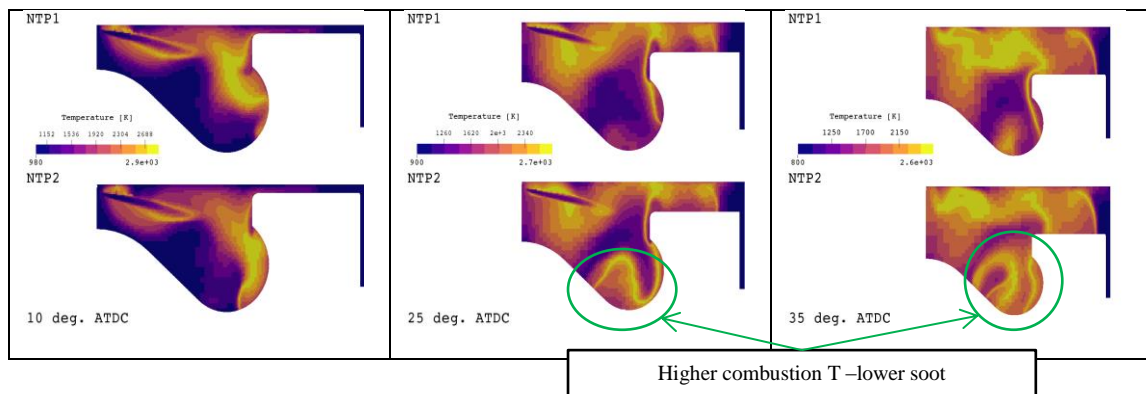


**Figure 14: Predicted in-cylinder temperature at three crank angles for NTP 1 (upper) and NTP 2 (lower) at 4000 rpm.**

Figure 15a shows the  $ISNO_x$  emissions from the engine at full load. A decrease in  $ISNO_x$  with NTP can be seen.  $ISNO_x$  mass predictions from the CFD are shown in Figure 15b. Again the trends shown in the experimental results are closely followed – with a general reduction in  $NO_x$  with NTP 2, at 1500, and 2000 rpm, but a relatively flat trend at 4000 rpm. Because  $NO_x$  is measured more directly than soot (via a chemiluminescence in the Horiba analyser) these measurements may be compared more directly.

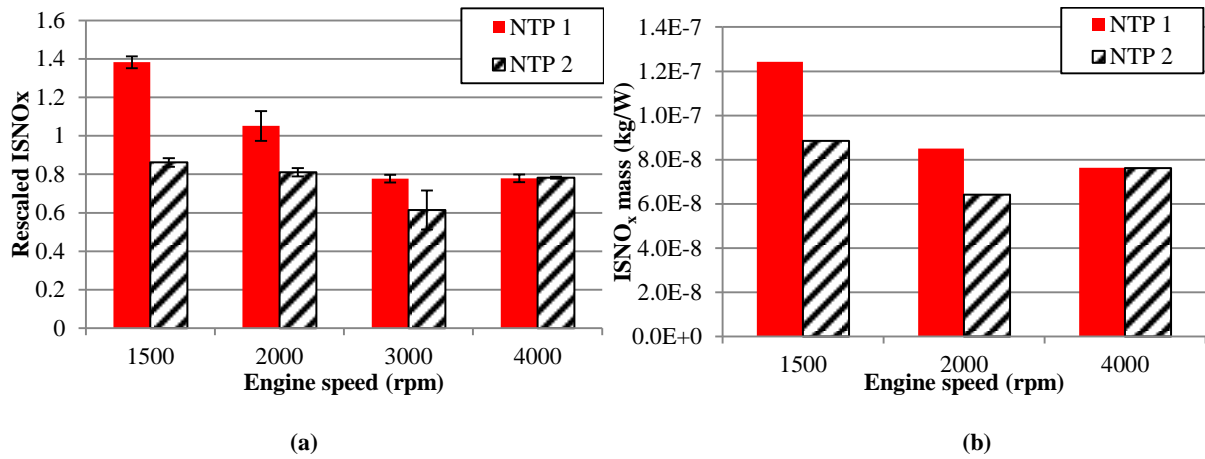
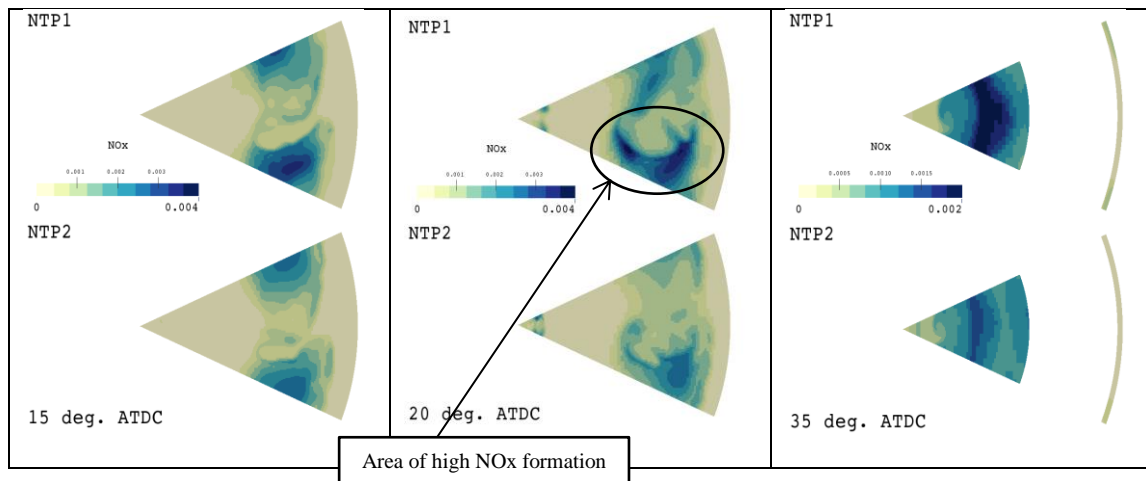
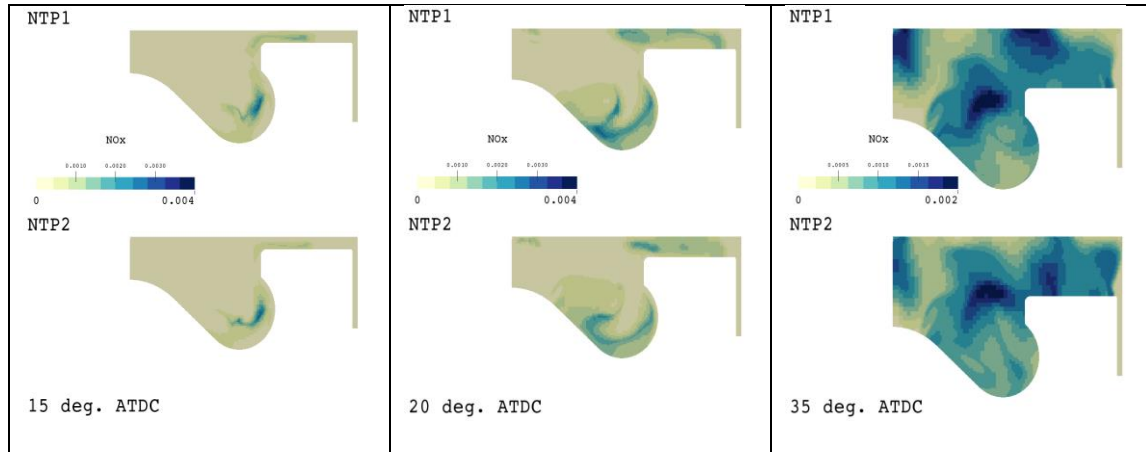


Figure 15: Measured ISNO<sub>x</sub> emissions (a) and CFD predicted ISNO<sub>x</sub> mass (b) at full load. The error bars correspond to  $\pm\sigma$ .

The in-cylinder CFD gives a good insight as to why the NO<sub>x</sub> trends are as they are in the experimental results. Figure 16 and Figure 17 show the in-cylinder NO<sub>x</sub> mass fraction and temperature respectively at 1500 rpm, full load. A significant increase in NO<sub>x</sub> formation is observed at NTP 1 at 20 CAD (Figure 16) which corresponds to an area of high temperature observed in Figure 17. This higher temperature is caused by the decreased vortex seen in the bowl with the interaction of the spray plume and the air motion at NTP 1 and a further penetration of this spray into the fire land and less entering the vortex in the bowl (compared to NTP 2), burning significantly hotter as a result.





**Figure 16: Predicted NO<sub>x</sub> mass fraction in cylinder at three crank angles for the standard bowl at NTP 1 (upper) and NTP 2 (lower) at 1500 rpm, full load.**

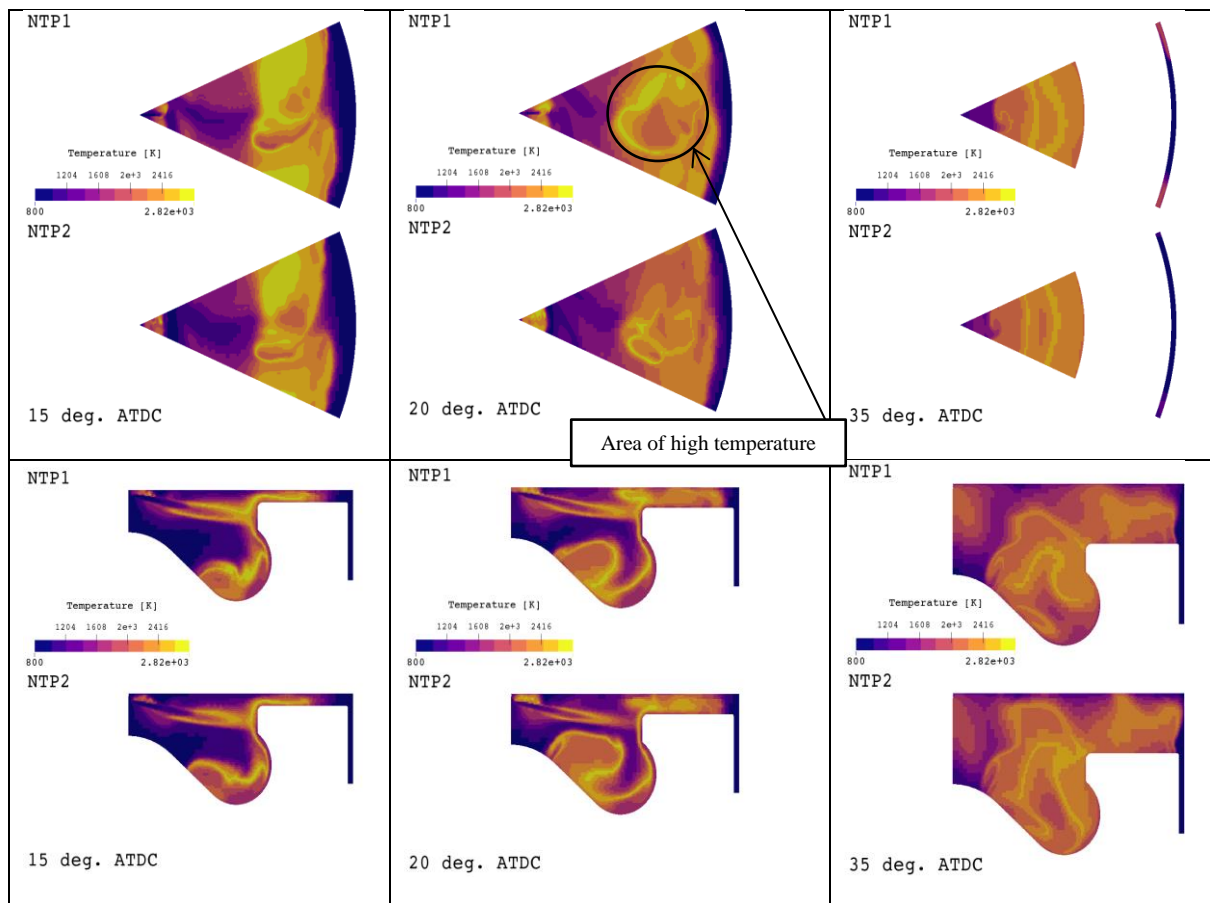


**Figure 17: Predicted in-cylinder temperature at three crank angles for the standard bowl at NTP 1 (upper) and NTP 2 (lower) at 1500 rpm, full load.**

Overall, the results demonstrate that the soot emissions can be reduced with NTP 2, without compromising other combustion parameters or NO<sub>x</sub> emissions. It is also possible that this observed soot reduction effect of NTP 2 might be able to be achieved by changing the injector angle or injection timing which, considering in cylinder clearances, may be a preferred



option, but would require further research. This sensitivity to a minor (0.5 mm) variation in NTP is particularly important as NTP could be changed through a vehicles' life, for example at service, or be affected by other manufacturing considerations.

## Conclusions

In this work we have used a well-validated CFD model to explain experimentally observed combustion and emissions trends from a high-speed diesel engine subject to small variations in Nozzle Tip Protrusion (NTP) of 0.5 mm. This study considers the effects of two NTPs using a standard re-entrant bowl shape, at two part load operating points and under full load operation at four engine speeds. The well validated CFD analysis provides essential physical insight into the details of the spray, mixing, and combustion processes at each operating point. The results show that:

- a significant amount of NO<sub>x</sub> and soot formation is occurring in the fire land, around the bowl lip.
- Both this NO<sub>x</sub> and soot formation can be reduced at NTP 2.
- Moving from NTP 1 to NTP 2 achieves a reduction in soot at full load and part load, by mixing the air and fuel better using the bowl vortex, without any significant NO<sub>x</sub> penalty, as the overall combustion temperatures remain similar – i.e. reducing soot formation overall rather than promoting soot oxidation.
- NTP 2 has no adverse effects on other combustion characteristics.

It is acknowledged that there might be alternative ways of achieving the same effect using injection timing or injector angle, such work is outside the scope of this paper. Such a minor change in NTP may occur through a vehicle lifetime, for example if the injectors were changed, and hence lead to a change in the observed NO<sub>x</sub> and soot emissions.

## Acknowledgements

The authors would like to thank Jaguar Land Rover Limited and University of Oxford John Fell fund for financial support.

The authors would also like to thank BP International for supplying the diesel fuel. The authors would like to thank Dave Richardson of Jaguar Land Rover for technical advice and support, and Liyah Dholiwar and the Department of Engineering Science technicians and maintenance teams for undertaking much of the engine testing and facilities support.

## References

1. SMMT, *New Car CO2 Report 2018*.
2. SMMT. *UK new car market declines in 2017 but demand still third highest in 10 years*. 2018; Available from: <https://www.smm.co.uk/2018/01/uk-new-car-market-declines-2017-demand-still-third-highest-10-years/>.
3. ICCT, *European Vehicle Market Statistics Pocketbook 2016/17*.
4. ICCT, *Estimated Cost of Emission Reduction Technologies for Light-Duty Vehicles*. 2012.
5. Yang, J., et al., *Single wall diesel particulate filter (DPF) filtration efficiency studies using laboratory generated particles*. Chemical Engineering Science, 2009. **64**(8): p. 1625-1634.

6. Salvat, O., P. Marez, and G. Belot, *Passenger Car Serial Application of a Particulate Filter System on a Common Rail Direct Injection Diesel Engine*. SAE Technical Paper 2000-01-0473, 2000.
7. ICCT, *NOx control technologies for Euro 6 Diesel passenger cars. Market penetration and experimental performance assessment*. 2015.
8. Hoard, J. and R. Hammerle, *Economic Comparison of LNT Versus Urea SCR for Light Duty Diesel Vehicles in US Market*, in *DEER Conference*. 2004: Coronado, California.
9. Pickett, L.M. and D.L. Siebers, *Soot in diesel fuel jets: effects of ambient temperature, ambient density, and injection pressure*. Combustion and Flame, 2004. **138**(1–2): p. 114-135.
10. Ehleskog, R., R. Ochoterena, and S. Andersson, *Effects of Multiple Injections on Engine-Out Emission Levels Including Particulate Mass from an HSDI Diesel Engine*. SAE Technical Paper 2007-01-0910, 2007.
11. Gill, K., et al., *In-cylinder Studies of Multiple Diesel Fuel Injection in a Single Cylinder Optical Engine*. SAE Technical Paper 2005-01-0915, 2005.
12. Montgomery, D. and R. Reitz, *Effects of Multiple Injections and Flexible Control of Boost and EGR on Emissions and Fuel Consumption of a Heavy-Duty Diesel Engine*. SAE Technical Paper 2001-01-0195, 2001.
13. O'Connor, J. and M. Musculus, *Post Injections for Soot Reduction in Diesel Engines: A Review of Current Understanding*. SAE International Journal of Engines, 2013. **6**(1): p. 400-421.
14. Han, Z., et al., *Mechanism of Soot and NOx Emission Reduction Using Multiple-injection in a Diesel Engine*. SAE Technical Paper 960633, 1996.
15. Yu, H., et al., *Numerical investigation of the effect of two-stage injection strategy on combustion and emission characteristics of a diesel engine*. Applied Energy, 2017.
16. d'Ambrosio, S. and A. Ferrari, *Diesel engines equipped with piezoelectric and solenoid injectors: hydraulic performance of the injectors and comparison of the emissions, noise and fuel consumption*. Applied Energy, 2018. **211**: p. 1324-1342.
17. Tauzia, X. and A. Maiboom, *Experimental study of an automotive Diesel engine efficiency when running under stoichiometric conditions*. Applied Energy, 2013. **105**: p. 116-124.
18. Han, S., J. Kim, and C. Bae, *Effect of air–fuel mixing quality on characteristics of conventional and low temperature diesel combustion*. Applied Energy, 2014. **119**: p. 454-466.
19. Miles, P.C. and Ö. Andersson, *A review of design considerations for light-duty diesel combustion systems*. International Journal of Engine Research, 2015. **17**(1): p. 6-15.
20. Ismail, R., et al., *Computational Investigation of the Effects of Piston Geometry on the Combustion Evolution in a Light Duty HSDI Engine*, in *ASME 2017 Internal Combustion Fall Technical Conference*. 2017, ASME: Seattle, WA, USA.
21. Lee, J., et al., *A characteristic study and optimization of in-cylinder configuration for particulate matters reduction in an off-highway diesel engine with mechanical fuel injection system*. Proceedings of the Institution of Mechanical Engineers, Part D: Journal of Automobile Engineering, 2017. **231**(6): p. 798-809.
22. Tonetti, M., et al., *Diesel Engine Technologies Evolution for Future Challenges*. 2017, SAE International.
23. Leach, F., et al., *The effect of a stepped lip piston design on performance and emissions from a high-speed diesel engine*. Applied Energy, 2018. **215**: p. 679-689.
24. Leach, F., et al., *Comparing the Effect of Fuel/Air Interactions in a Modern High-Speed Light-Duty Diesel Engine*. SAE Technical Paper 2017-24-0075, 2017.
25. *British Standards BS EN 590 Diesel, Requirements and Test Methods*. 2009.
26. Papaioannou, N., et al., *Evaluation of EGR techniques on a HSDI diesel engine using first law analysis*. Proceedings of the Institution of Mechanical Engineers, Part D: Journal of Automobile Engineering, 2018.
27. Richards, K.J., P.K. Senecal, and E. Pomraning, *CONVERGE (v2.3)*. Convergent Science, 2016.
28. Senecal, P.K., et al., *Grid-Convergent Spray Models for Internal Combustion Engine CFD Simulations*. 2012(55096): p. 697-710.
29. Moiz, A.A., et al., *Experimental and Numerical Studies on Combustion Model Selection for Split Injection Spray Combustion*. SAE Technical Paper 2015-01-0374, 2015.
30. Colin, O. and A. Benkenida, *The 3-zones extended coherent flame model (ECFM3Z) for computing premixed/diffusion combustion*. Oil & Gas Science and Technology, 2004. **59**(6): p. 593-609.
31. Bohbot, J., et al., *An Innovative Approach Combining Adaptive Mesh Refinement, the ECFM3Z Turbulent Combustion Model, and the TKI Tabulated Auto-Ignition Model for Diesel Engine CFD Simulations*. SAE Technical Paper 2016-01-0604, 2016.
32. Orszag, S.A., et al., *Renormalization group modeling and turbulence simulations*. Near-wall turbulent flows, 1993: p. 1031-1046.
33. Han, Z. and R.D. Reitz, *A temperature wall function formulation for variable-density turbulent flows with application to engine convective heat transfer modeling*. International Journal of Heat and Mass Transfer, 1997. **40**(3): p. 613-625.
34. Reitz, R.D. and R. Diwakar, *Structure of high-pressure fuel sprays*. 1987, SAE Technical Paper.
35. Reitz, R.D. and F. Bracco, *Mechanisms of breakup of round liquid jets*. Encyclopedia of fluid mechanics, 1986. **3**: p. 233-249.
36. O'Rourke, P.J. and A.A. Amsden, *The TAB method for numerical calculation of spray droplet breakup*. 1987, Los Alamos National Lab., NM (USA).
37. Schmidt, D.P. and C.J. Rutland, *A New Droplet Collision Algorithm*. Journal of Computational Physics, 2000. **164**(1): p. 62-80.
38. Amsden, A.A., P.J. O'Rourke, and T.D. Butler, *KIVA-II: A computer program for chemically reactive flows with sprays*, in *Other Information: Portions of this document are illegible in microfiche products*. 1989.

39. Heywood, J.B., *Internal combustion engine fundamentals*. Vol. 930. 1988: McGraw-hill New York.
40. Hiroyasu, H. and T. Kadota, *Models for Combustion and Formation of Nitric Oxide and Soot in Direct Injection Diesel Engines*. SAE Technical Paper 760129, 1976.
41. Nagle, J. and R. Strickland-Constable. *Oxidation of Carbon between 1000-2000 C.* in *Proceedings of the fifth carbon conference*. 1962. Pergamon Press London.

## Definitions and abbreviations

<b>CA b(a)TDC</b>	Crank Angle before (after) Top Dead Centre
<b>CAD</b>	Crank Angle Degrees
<b>CFD</b>	Computational Fluid Dynamics
<b>DOC</b>	Diesel Oxidation Catalyst
<b>DPF</b>	Diesel Particulate Filter
<b>EGR</b>	Exhaust Gas Recirculation
<b>HSDI</b>	High Speed Direct Injection
<b>IMEP</b>	Indicated Mean Effective Pressure
<b>ISFC</b>	Indicated Specific Fuel Consumption
<b>NO<sub>x</sub></b>	Indicated Specific Nitrogen Oxides
<b>LNT</b>	Lean NO <sub>x</sub> Trap
<b>nIMEP</b>	Net Indicated Mean Effective Pressure
<b>NO<sub>x</sub></b>	Nitrogen Oxides
<b>NTP</b>	Nozzle Tip Protrusion
<b>PM</b>	Particulate Matter
<b>SCR</b>	Selective Catalytic Reduction
<b>TDC</b>	Top Dead Centre
<b>TKI</b>	Tabulated Kinetic Ignition
<b>TP</b>	Test Point